

Tuning Molecule–Surface Interactions with Sub-Nanometer-Thick Covalently Bound Organic Monolayers

Nicholas Camillone III* and Theodore R. Pak

Chemistry Department, Brookhaven National Laboratory, Upton, New York 11973

Kaveh Adib and Richard M. Osgood, Jr.

Department of Applied Physics, Columbia University, New York, New York 10027

Received: January 31, 2006; In Final Form: April 14, 2006

Measurements of the thermal desorption of methyl bromide (MeBr) from bare and RS-functionalized GaAs-(110), where R = CH₃ and CH₃CH₂, reveal marked systematic changes in molecule–surface interactions. As the thickness of the organic spacer layer is increased, the electrostatic MeBr–GaAs(110) interaction decreases, lowering the activation energy for desorption, E_d , as well as decreasing the critical coverage required for nucleation of bulklike MeBr. On the CH₃CH₂S-functionalized surface, E_d is lowered to a value roughly equal to that for desorption from three-dimensional (3-D) clusters; because the kinetics of desorption of isolated molecules differs from that for desorption from clusters, desorption of isolated molecules from the organic surface occurs at a lower temperature than desorption from the clusters. Thus, the “monolayer” desorption wave occurs at a lower temperature than the “multilayer” desorption wave. These results illustrate the role that organic chain length in nanometer-scale thin films can play in alteration of the delicate balance of interfacial interactions.

Introduction

A key challenge in nanoscience is understanding how deliberate tailoring of materials at nanometer-length scales can lead to novel and/or enhanced functionalities.¹ Understanding the physical bases for such changes in functionalities requires atomic-level understanding of the interactions among molecules and between molecules and nanoscale objects. Systematic experimental approaches to achieving such understanding involve decomposing the problem into constituent parts or examining interactions as a function of dimensionality. A logical point to conduct such studies is to examine interactions between molecules and single-molecule-thick thin films on planar surfaces.

A study of molecular layers on planar surfaces is a useful starting point² because understanding the stability and structure of thin atomic and molecular layers has implications in many areas of thin-film science and engineering. For example, monolayer and ultrathin multilayer films have been used as the basis for the study of phenomena as diverse as wetting,³ charge attachment to^{4,5,6} and transfer through^{7,8,9} molecular thin films, charge transfer in electro-chemical systems,¹⁰ organic overlayer growth and ordering,^{11,12} two-dimensional (2-D) melting,¹³ and the formation of nanoparticles using buffer layers^{14,15,16} and reactive layers.¹⁷ One class of monolayer, organic self-assembled monolayers (SAMs), has been the subject of numerous studies dealing with potential applications in research fields as diverse as molecular recognition, photoresists for microstamp-lithography, surface biology and biochemistry, chemical force microscopy, surface passivation, alignment of liquid crystals, and pH-sensing devices.² In many instances, molecular layers act,

in part, as “spacer layers”, intervening, either actively or passively, between the surface of a solid and the physicochemical phenomena occurring at or near its surface. Such nanoscale spacer layers can range from simple noble gases to SAMs of functionalized long-chain organothiols. Often it is important that the molecules comprising the spacer layer be covalently bound to the substrate surface because, for single-molecule-thick spacer layers, more loosely bound species, e.g., noble-gas atoms, cannot prevent percolation of more strongly bound, e.g., dipolar molecules, to the substrate surface.¹⁸ In all cases, it is important to understand molecular interactions at the surfaces of the spacer layers to perform and interpret the experiments involving them.

Studies of the variation in molecular adsorption behavior with molecular configuration on organofunctionalized solid surfaces, such as SAM layers, have involved the use of various techniques to determine overlayer structure and binding energetics including TPD, infrared reflection–absorption spectroscopy,^{19,20} standard²¹ and angle-resolved²² X-ray photoelectron spectroscopy, sum-frequency generation (SFG) spectroscopy,²³ and He diffraction.^{24,25} These studies range from the examination of simple atomic adsorbates, such as noble gases,²⁴ to strongly hydrogen-bonded molecules, such as water, to long-chain thiols²⁵ or alcohols^{21,22} of varying chain length. Such experiments have explored the dependence of overlayer structure and desorption kinetics on the balance struck among dispersion interactions, dipolar forces, and hydrogen bonding. These studies have generally confirmed the intuitive understanding that strongly interacting adsorbates, i.e., those that interact via dipole–dipole or hydrogen-bonding interactions, wet hydrophilic surfaces but not hydrophobic surfaces.

We report here the results of a relatively simple experimental approach to probing changes in molecular interactions due to modification of the interface by introducing sub-nanometer-thick

* To whom correspondence should be addressed. E-mail: nicholas@bnl.gov.

organic spacer layers between the molecule and the solid surface. The experiments involve temperature-programmed desorption (TPD) of methyl bromide (MeBr) from bare and organosulfur-functionalized GaAs(110). MeBr serves as a “probe” species, and CH₃S- and CH₃CH₂S- serve as relatively robust spacer layers. We have chosen this model system for several reasons. First, the GaAs(110) surface is relatively easily and reproducibly prepared. Also, MeBr is a well-characterized molecule, as are its interactions with the GaAs(110) surface.^{26,27} These earlier studies showed that the adsorption of MeBr on GaAs(110) is molecular, with a binding energy (~ 0.5 eV) falling at the border between chemisorption and physisorption. Ab initio calculations indicated that a small amount of charge, approximately 0.05 electron, is transferred from the Br to the Ga, likely the result of overlap of a Br lone pair with the empty Ga *p* orbital. More striking, however, is the charge redistribution experienced by both the molecule and surface atoms at the binding site; a polarizing electrostatic interaction acts to increase the MeBr dipole by about 25%. This charge redistribution is mirrored in the Ga and As atoms at the binding site, resulting in strong dipole–dipole interactions between adsorbate and surface dipoles.²⁷ Thus, the insertion of a nonpolar spacer layer would be anticipated to decrease the adsorbed-molecule–surface interaction; increasing the thickness of the spacer layer would act to further decrease the strength of this interaction. Note that both the GaAs surface and a nonpolar surface layer would also contribute an additional binding term due to the induced-dipole–induced-dipole attraction (the so-called dispersion or London forces). The *change* in the dispersion interaction, i.e., the difference between the MeBr–CH₃S/GaAs(110) and MeBr–CH₃CH₂S/GaAs(110) dispersion interaction, is expected to be considerably smaller in magnitude than the change in the MeBr–GaAs(110) electrostatic interaction.

Our choice of organosulfur compounds as spacer-layer molecules was motivated by studies of their adsorption on the (110)²⁸ and (100)^{29,30,31,32} faces of this particular semiconductor and governed by several considerations. First, to conveniently and reproducibly prepare high-purity spacer layers in UHV, the constituent molecules should have a vapor pressure in or near the Torr range. The molecules should be nonpolar yet have a chemical affinity for the GaAs surface. They should also comprise a homologous series, such that their length may be varied. The end of the molecule exposed to the vacuum should be chemically inert with respect to the dipolar “probe” molecule. In addition, with a view toward planned future experiments involving UV photoinitiated chemistry at the organic spacer layer surface, once bound to the surface, the spacer-layer molecules themselves should be resistant to UV-induced photochemistry. Covalently bound thiolates, such as those that have been used with great success to form well-ordered SAMs, particularly on gold surfaces,³³ meet all of these criteria.

To prepare thiolate spacer layers in these experiments, it was necessary to dissociatively chemisorb disulfide compounds. When dosed in UHV, the alkyl disulfides form robust covalently bound monolayers on GaAs(110), as compared to more loosely bound thiols and dialkyl sulfides. The variation in the molecule–GaAs(110) bond strength for these three classes of organosulfur compounds²⁸ is illustrated by comparison of TPD spectra of the representative organosulfur molecules methanethiol (CH₃SH), dimethyl sulfide [(CH₃)₂S], and methyl disulfide [(CH₃)₂S₂], abbreviated MeSH, Me₂S, and Me₂S₂, respectively. As shown in Figure 1, their TPD spectra indicate distinctive adsorption/desorption behavior. MeSH adsorbs intact and exhibits well-defined first- and second-monolayer desorption peaks shown

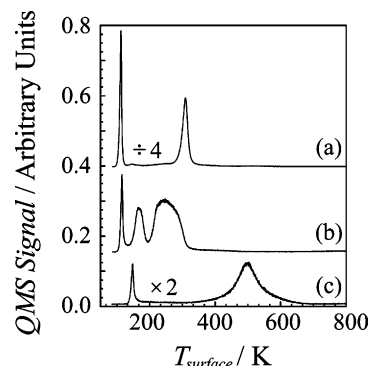


Figure 1. Comparison of the temperature-programmed desorption spectra of (a) MeSH, (b) Me₂S, and (c) Me₂S₂ from the GaAs(110) surface. The spectra are displaced vertically for clarity and scaled as indicated.

in Figure 1a. These peaks have very different activation energies of desorption, E_d . For the first and second monolayers, we estimate E_d to be 0.81 and 0.34 eV, respectively.²⁸ The disparity in these values indicates that the MeSH–GaAs(110) bond is stronger than would be expected were it physisorbed, suggesting some degree of molecular chemisorption, perhaps due to a hydrogen-bonding interaction. Me₂S also adsorbs molecularly, but exhibits at least two and possibly three distinct desorption peaks in the first monolayer (Figure 1b),²⁸ with the most strongly bound having $E_d = 0.79$ eV, suggesting molecular chemisorption similar to that of the thiol.

In contrast, Me₂S₂ is unique among the three methyl organosulfur molecules in that it adsorbs dissociatively; the TPD data (Figure 1c) suggest that Me₂S₂ dissociates to form two methyl thiolate moieties. Upon heating, the surface-bound thiolates react to evolve Me₂S, which desorbs at ~ 500 K, corresponding to a value for E_d of 3.2 eV, using Redhead’s method³⁴ assuming second-order kinetics.²⁸ Because it dissociates, the disulfide yields surface species that are significantly more strongly bound to GaAs than do MeSH or Me₂S. Furthermore, the absence of the ~ 500 K peak from the TPD spectrum of MeSH is consistent with our assertion that the S–H bond remains intact when these molecules adsorb at ~ 90 K.^{28,35} In addition, separate surface photochemical studies of MeSH on GaAs(110) have shown that UV irradiation efficiently cleaves the S–H bond.³⁵ In contrast, thiolates on GaAs(110) produced by Me₂S₂ exposure show a cross section for UV photoreaction that is more than an order of magnitude smaller than that of MeSH,³⁵ further illustrating the robustness of monolayers grown with dimethyl sulfide. More details on the chemistry of the three representative organosulfur molecules on GaAs(110) can be found in ref 28. The thermal chemistry of Me₂S₂ on GaAs(110) is reviewed below for the purpose of comparison with new TPD results for (CH₃CH₂S)₂ (abbreviated Et₂S₂).

Here, we report the in-vacuo deposition of the two shortest alkyl disulfides for use as spacer layers of differing thickness, allowing studies of MeBr adsorption atop organic thin films at a controlled distance from the underlying GaAs substrate. We have performed our experiments at the short-chain limit, using spacer-layer molecules containing one and two carbon atoms, where we expect the changes in molecule–surface interactions to be the most significant. We find that the MeBr-adsorption growth modes are markedly modified from those on the bare surface and that as the distance between the GaAs surface and the MeBr increases, the activation energy of desorption for the MeBr at low coverages decreases, indicating a decrease in the strength of the surface–adsorbate interaction. Furthermore, as

the surface–adsorbate interaction strength decreases, the *relative* strength of the adsorbate–adsorbate lateral interactions is enhanced. This is most dramatically seen for MeBr adsorption atop the spacer layer formed by Et₂S₂ chemisorption, in which case desorption of MeBr molecules adsorbed directly atop the spacer layer occurs at *lower* temperature than that of multilayer MeBr.

Experimental Section

The experiments are conducted in a surface analysis system, which has been described elsewhere.³⁶ The system consists of a multilevel UHV vessel (base pressure $\sim 2 \times 10^{-10}$ Torr) equipped with a low-energy electron diffraction (LEED) system, a quadrupole mass spectrometer (QMS), an effusive-beam pinhole gas doser, and a crystal manipulator cooled with liquid nitrogen (LN₂). For temperature-programmed desorption (TPD) experiments, the crystal is heated by passing a computer-controlled current through the Mo foil on which the crystal is mounted so as to raise the crystal temperature at a constant rate of 2.5 K/s. The QMS is housed in a separate, differentially pumped chamber that is joined to the surface-analysis chamber by a 3-mm aperture. The doser consists of a ~ 0.01 -mm aperture mounted ~ 10 cm upstream of the end of a stainless steel tube with an inside diameter of 6 mm. This arrangement affords TPD-desorbate-flux measurements with low background levels. The temperature ramp is computer controlled using a proportional-integral-differential feedback loop. Data are collected from the output of the continuous-dynode electron multiplier of the QMS; each point is the average over 100 samples measured at a rate of ~ 1 kHz, and the data are presented as acquired without further smoothing.

The $1 \times 1 \times 0.1$ cm³ GaAs crystals [Atramet, (110) orientation, n-type, Si-doped, 1.4×10^{17} cm⁻³ carrier concentration] are cleaned after their introduction into the UHV system by cycles of Ar⁺ sputtering and annealing at 840 K. The surface order of the clean crystal is judged by the observation of a sharp, intense, low-background-level LEED pattern at room temperature and low incident-electron energies (~ 20 – 30 eV).

Organosulfur monolayers were formed by the following protocol. First, the methyl disulfide [(CH₃S)₂, Aldrich, 99.5%] and ethyl disulfide [(CH₃CH₂S)₂, Aldrich, 99%] were purified by removal of volatile contaminants by freeze–pump–thaw cycles. The crystal was exposed to the effusive flux of Me₂S₂ (Et₂S₂) for 4 min (10 min) at 300 K and then allowed to cool over a period of approximately 2 min to 100 K while still under the flux. The flux was then terminated, and the methyl thiolate (ethyl thiolate) film was annealed by ramping to 300 K (350 K). Deposition during cool-down encouraged rapid monolayer saturation, and the postdeposition annealing desorbed any molecules in excess of a saturated monolayer. We believe that the 300–350 K deposition temperature is high enough to promote adsorbate surface diffusion, and TPD measurements indicate that it is low enough to prevent significant desorption of the dissociatively adsorbed thiolates. Our procedure was found to provide a film relatively free of defects as determined by the absence of defect-related desorption signatures (low-intensity peaks at temperatures above that of the monolayer desorption wave) in subsequent MeBr TPD spectra. Further work, involving scanning probe microscopy or surface diffraction, should be performed to quantify the order of these films.

Methyl bromide (MeBr, Aldrich, 99.5%) was used without further purification. Overlayers were grown by exposing the LN₂-cooled crystal to the flux generated by expanding the MeBr through the pinhole doser from a fixed volume at a known initial

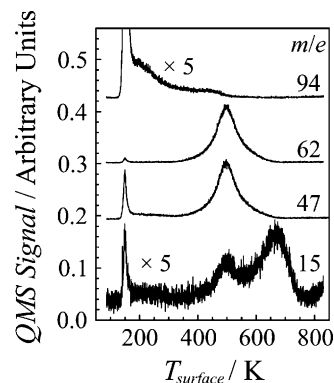


Figure 2. TPD spectra for Me₂S₂ from GaAs(110). Desorption waves for the intact molecule from the second layer at ~ 150 K, and for Me₂S at ~ 500 K, are readily identified. The spectra are displaced vertically for clarity and scaled as indicated. The *m/e* values of 94, 62, 47, and 15 correspond to Me₂S₂⁺, Me₂S⁺, MeS⁺, and Me⁺ ions, respectively.

pressure, typically 5 Torr, for a predetermined period of time (~ 80 s was found to be equivalent to 1 ML). The volume behind the pinhole can be abruptly (~ 1 s) filled and evacuated, providing a well-defined exposure period. This method affords coverage reproducibility better than 2% of a monolayer. For the experiments involving the adsorption of MeBr on the EtS monolayers on GaAs(110), the routinely achieved surface base temperature of ~ 90 K was not cold enough to prevent annealing of the MeBr layer (as discussed in further detail below). Therefore, it was necessary to pump on the space above the LN₂ in the cryostat with a mechanical pump to lower the LN₂ boiling point. With this technique, we were able to achieve surface temperatures below 80 K. For MeBr adsorption on bare and MeS-covered GaAs(110), the routinely achieved ~ 90 K base temperature was sufficiently low.

Results

A. Chemistry of Organosulfur Molecular Spacer Layers.

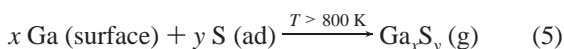
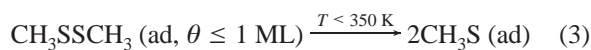
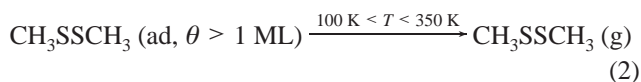
The first phase of our experiments involved understanding the chemistry of the formation of the alkyl-sulfide spacer layers by reaction of the corresponding alkane disulfides, i.e., Me₂S₂ or Et₂S₂ on the GaAs(110) surface. In this section, we present TPD studies of these molecules after adsorption on GaAs(110) at ~ 90 K. More extensive Me₂S₂ desorption spectra have been published elsewhere,²⁸ and these data are presented here for the purpose of comparison with the more recent Et₂S₂ spectra.

Figure 2 shows selected spectra collected during the TPD of Me₂S₂ from GaAs(110) recorded with the QMS set to monitor species with mass-to-charge (*m/e*) ratios equal to 94, 62, 47, and 15. Two distinct low-temperature features are discerned: a well-developed peak at ~ 150 K and a low-intensity tail, comprised of two broad features, trailing off to ~ 450 K. The well-developed peak is assigned to molecular desorption of the physisorbed Me₂S₂ bilayer. The low-intensity tail is assigned to desorption from defects in the substrate and/or the nascent chemisorbed monolayer beneath the second layer. Neither the molecules comprising the peak at 150 K nor those in the higher temperature tail have undergone a chemical transformation at the surface. This conclusion is supported by the fact that the ratios of the intensities of these desorption features measured at *m/e* values corresponding to those of the principle daughter ions of Me₂S₂ are in close agreement with the ratios measured by directly leaking Me₂S₂ into the QMS. In addition, application of the Habenschaden and Küppers (HK)³⁷ leading-edge analysis to these data give the activation energy of desorption for the

peak at ~ 150 K to be in reasonable agreement with the bulk heat of vaporization.^{28,38}

In contrast to the data for the desorption of physisorbed Me_2S_2 , the desorption waves at significantly higher temperatures indicate that a chemical reaction between the surface and molecules in the first monolayer has occurred. Specifically, we observe two peaks in the $m/e = 15$ desorption signal; one at ~ 500 K and a second at ~ 670 K. As explained in further detail in ref 28, these features are assigned, respectively, to: (1) associative desorption of chemisorbed methyl thiolates (MeS) resulting in the elimination of a sulfur atom to yield dimethyl sulfide (Me_2S), and (2) decomposition of the methyl thiolates resulting in the desorption of CH_3 . Both processes result in the segregation of sulfur to the GaAs surface. An analysis based on the cracking patterns of the relevant species allowed us to estimate the relative yield of the two processes to be 95 and 5%, respectively.²⁸ Furthermore, the Me_2S desorption feature (see Figure 2, $m/e = 62$) is generally symmetric, and analyses of the coverage dependence (data shown in ref 28) indicates that the evolution of Me_2S follows second-order kinetics.²⁸ Note that in a separate set of experiments, we found that desorption of Me_2S following UV-induced cleavage of the MeS–H bond followed the same kinetics.³⁵ The weight of this evidence argues in favor of the conclusion that the majority of the Me_2S_2 molecules in the first monolayer dissociate to form a methyl thiolate (MeS) monolayer.

We can summarize the above description of Me_2S_2 chemistry on GaAs(110) with the following equations:



The first equation describes the initial physisorption. The second describes thermal desorption of molecules from the second or higher molecular layer. The need for thermal activation for the third step is not unambiguously established; the evidence suggests that the reaction proceeds spontaneously at some temperature below ~ 350 K.²⁸ Reaction 4 describes the subsequent thermal reaction of the trapped MeS species to evolve desorbed Me_2S at ~ 500 K and produce a surface-bound sulfur species. Evidence of the sulfur product in reaction 4 is found in the desorption of a gallium sulfide moiety, reaction 5, observed at $m/e = 101$ with an onset of ~ 780 K (data not shown).

The desorption spectra for Et_2S_2 evidence a very similar type of physicochemical interaction between Et_2S_2 and GaAs(110) as was observed for Me_2S_2 . Figure 3 shows molecular-desorption peaks for the parent molecule at ~ 175 K, and the evolution of Et_2S ($m/e = 90$) peaked at ~ 480 K. These data indicate that the Et_2S_2 undergoes the same dissociative adsorption and associative sulfur-elimination processes as the methyl homologue. As in the case of Me_2S_2 , the desorption of ethyl fragments at high temperature is clearly a minority process compared to the associative sulfur-elimination process that results in the evolution of Et_2S . Likewise, as in the case of Me_2S_2 , we expect that the production of surface-bound ethyl fragments may be

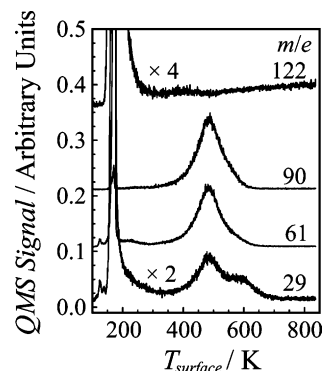


Figure 3. TPD spectra for Et_2S_2 from GaAs(110). Desorption waves for the intact molecule from the second layer at ~ 175 K, and for Et_2S at ~ 480 K, are readily identified. The spectra are displaced vertically for clarity and scaled as indicated. The m/e values of 122, 90, 61, and 29 correspond to Et_2S_2^+ , Et_2S^+ , EtS^+ , and Et^+ ions, respectively.

due to decomposition at defect sites on the GaAs(110) and/or decomposition of single EtS adsorbates that do not encounter other EtS adsorbates during the temperature ramp and are thus unable to react to evolve Et_2S .

The desorption of ethyl fragments at ~ 600 K is of some note, because it provides further insight into the surface chemistry through comparison to thermal desorption observed following the generation of surface-bound ethyl fragments by a different process. Specifically, in previous work we have reported the UV photoinduced dissociation of EtBr on GaAs(110).³⁹ In these experiments, the Et–Br bond cleavage is induced by exposure to UV light, and the ejected and trapped photofragments are monitored with the QMS during UV exposure and in post-irradiation TPD, respectively. In these measurements, the surface-bound ethyl fragments generated by UV exposure were found to desorb at the same temperature (600 K) as the ethyl fragments created by thermal reaction of Et_2S_2 with GaAs(110). This agreement supports our assignment of the 600 K feature in Figure 3 as surface-bound ethyl fragments and argues strongly in support of the conclusion that the kinetics of the high-temperature ethyl desorption wave is limited by the cleaving of the Et–GaAs bond following decomposition of the molecule at the surface, and not by the decomposition process itself.

Previously, in our study of $\text{Me}_2\text{S}_2/\text{GaAs}(110)$, we were unable to draw similar conclusions regarding the production of surface-bound methyl fragments because UV-induced dissociation of MeBr on GaAs(110) does not leave measurable quantities of methyl fragments bound to the surface.³⁹ However, we have been able to observe surface-bound methyl fragments on GaAs(100).⁴⁰ In light of the agreement of the desorption temperatures for the ethyl fragments generated thermally from Et_2S_2 and photochemically from EtBr, we now believe that the agreement between the ~ 670 K desorption temperature for methyl fragments created on GaAs(100) by UV-induced MeBr dissociation and on GaAs(110) by thermal Me_2S_2 reaction indicates that the kinetics of the high-temperature methyl desorption wave is limited by the cleaving of the Me–GaAs bond following decomposition of the molecule at the surface, and not by the decomposition process itself.

The facts that (1) the ethyl desorption peak occurs ~ 70 K lower in temperature than that of the methyl, and (2) the Et_2S peak occurs ~ 16 K lower than that of the Me_2S can be explained by consideration of the C–S bond strengths reported for the molecules MeSH, Me_2S_2 , EtSH, and MeS_2Et . In both homologous pairs, i.e., MeSH/EtSH and $\text{Me}_2\text{S}_2/\text{MeS}_2\text{Et}$, the Et–S bond is found to be ~ 4 kcal/mol (0.17 eV) weaker than the

corresponding Me–S bond.⁴¹ Assuming that the bond strength between the organic moiety and the GaAs surface shows a similar behavior, one would expect the ethyl fragment to desorb at a temperature lower than the methyl. On the same basis, cleavage of the Et–S bond during the molecular rearrangement to form Et₂S from 2 EtS–GaAs(110) would be expected to occur at temperatures somewhat lower than that for Me–S cleavage to form Me₂S from 2 MeS–GaAs(110), resulting in a lower desorption peak temperature for the Et₂S product compared to that for the Me₂S. This behavior is distinct from that of both physisorbed and chemisorbed sulfur-containing hydrocarbons on Au(111); desorption enthalpies of the physisorbed species *increase* with increasing molecular size, closely tracking the bulk heats of vaporization, whereas those of the chemisorbed species are *independent* of chain length.⁴² In contrast, our results indicate that in the cases of the ethyl and methyl fragments and the Et₂S and Me₂S products desorbing from GaAs(110), the energetics are not dominated by attractive lateral interactions among adsorbates, but rather by the strength of the adsorbate–surface bond, and the strength of that bond is greater for the Me species than for the Et species.

B. Tuning Molecule–Surface Interactions. Our presentation of the MeBr TPD studies begins with results for adsorption on the clean GaAs(110) surface to establish a basis for comparison with adsorption on the organo-functionalized surfaces. Next, we present TPD measurements of MeBr adsorbed on CH₃S- and CH₃CH₂S-functionalized GaAs(110), hereafter abbreviated MeS/GaAs(110) and EtS/GaAs(110), respectively. We detail the marked and systematic changes that we observe in the MeBr desorption and consider their implications regarding how tuning the molecule–surface interactions affects the structure and growth-mode of the MeBr overlayer.

C. MeBr Adsorption on Bare GaAs(110). Previous studies have examined the adsorption of MeBr on GaAs(110).²⁶ In these experiments, as in the current work, dosing was accomplished at ~85 K, and the adsorbed layer was, except for limited reactions at defect sites, comprised of the intact molecule bound to the surface and oriented by strong electrostatic forces.^{27,43,44} Growth was believed to proceed essentially stepwise, layer-by-layer, from monolayer through trilayer. The activation energy for desorption of the monolayer was found to be coverage dependent, decreasing with increasing coverage due to repulsive dipole–dipole forces among the surface-aligned molecular dipoles.^{26,45} At the limit of zero coverage, a value for E_d of 0.47 eV was derived using Redhead’s method.³⁴ In the present experiments, for the purpose of comparison with results for the organofunctionalized surfaces when the desorption order is not known a priori (see below), we have used the leading edge³⁷ of the desorption wave to determine E_d at a given coverage. For reference, we note that at a coverage of 0.3 ML, the HK leading edge analysis gives E_d equal to 0.53 eV for MeBr desorption from the bare GaAs(110) surface.

Figure 4 shows TPD spectra collected at several values of coverage from 0.08 to 2.8 ML. There are three salient features to notice. First, peaks corresponding to monolayer, bilayer, and trilayer desorption are clearly distinguished. Second, the onset of growth of the bilayer desorption feature is not observed until the monolayer feature is close to saturation. Third, the shift in the position of the peak of the monolayer desorption wave to lower temperature with increasing coverage is obvious. The position of the peak in the monolayer desorption wave as a function of coverage is plotted in Figure 5a. We will refer to these data, along with those for the organofunctionalized surfaces (Figure 5b,c), in subsequent sections of this paper to

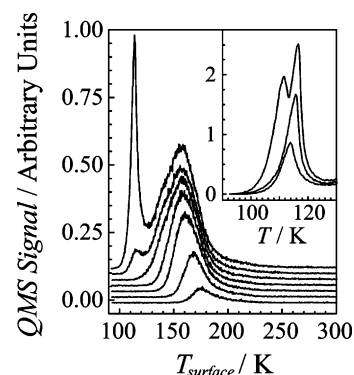


Figure 4. TPD spectra for MeBr from bare GaAs(110). Coverages are 0.08, 0.23, 0.46, 0.62, 0.77, 0.93, and 1.4 ML, from bottom to top. The spectra are displaced vertically for clarity. (Inset) Low-temperature range of TPD spectra measured at higher coverage. Coverages are 1.4, 1.9, and 2.8 ML, from bottom to top. Note that the range of the temperature scale of the inset is smaller than that of the main plot.

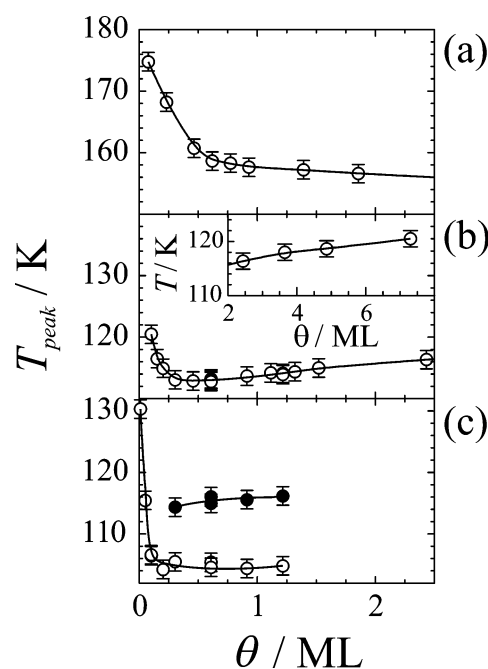


Figure 5. Monolayer desorption peak temperature versus coverage for MeBr from (a) bare GaAs(110), (b) MeS/GaAs(110), and (c) EtS/GaAs(110) at coverages in the 0–2 ML regime. The inset of (b) shows the behavior at higher coverage for desorption of MeBr from MeS/GaAs(110). The solid lines are guides to the eye.

quantitatively compare the coverage dependencies of the MeBr desorption features on the three surfaces examined in these experiments. With regard to the desorption behavior of the first monolayer of MeBr from the bare GaAs(110) surface, Figure 5a shows a sharp initial shift in the position of the monolayer desorption wave peak, with a slope of $\sim(-36)$ K/ML in the 0–0.5 ML range. The rate of the shift transitions in the 0.5–1.0 ML range to a much shallower slope of $\sim(-1.3)$ K/ML near saturation coverage, a weak trend compared to our estimated uncertainty (± 1.5 K) in determining the peak position and the relatively narrow coverage range over which the measurements were made.

To quantify the growth, the TPD spectra were analyzed by separating the integrated intensity under the TPD curves into the contributions due to the monolayer, bilayer, and trilayer. In this analysis, the total integrated intensity was found to increase linearly throughout the coverage range explored here, indicating

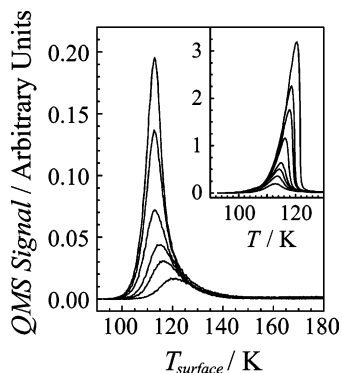


Figure 6. Coverage dependence of the desorption spectra of MeBr from MeS/GaAs(110) in the low-coverage regime. Coverages are 0.10, 0.15, 0.20, 0.30, 0.46, and 0.61 ML, from bottom to top. (Inset) Coverage dependence of the desorption spectra of MeBr from MeS/GaAs(110) in the high-coverage regime. Coverages are: 0.61, 0.91, 1.32, 1.52, 2.43, 3.65, 4.87, and 7.30 ML.

a constant sticking coefficient. The monolayer, bilayer, and trilayer intensities exhibited a layer-by-layer growth modality that was not completely ideal: the bilayer began to grow after the monolayer was $\sim 70\%$ complete, and the trilayer began to grow after the bilayer was $\sim 70\%$ complete. The saturation value for the monolayer was used to define single monolayer coverage; the 1 ML exposure-time equivalent, namely the time required to expose the surface to a fluence of molecules equal to 1 ML, is used throughout this work as the definition for 1 ML coverage.

D. MeBr Adsorption on MeS/GaAs(110). Figure 6 displays the coverage dependence of the TPD spectra of MeBr desorbing from a Me₂S₂-modified GaAs(110) surface, i.e., a surface functionalized with a MeS monolayer. As expected, the TPD data show some significant differences in the MeBr desorption behavior compared to that found for the bare GaAs(110) surface. There are also some similarities between the two data sets. For example, note that the desorption peaks have a comparable temperature width to those for the bare GaAs surface, suggesting that the underlying MeS layer is uniform and of good quality. Notice also that for coverages less than ~ 0.6 ML, the desorption peak shifts to lower temperature with increasing coverage, as was true in the case of the bare GaAs, cf. Figure 5a,b. Though the decrease in the value of the peak temperature is not linear with coverage, the rate of the decrease at coverages < 0.25 ML is roughly -54 K/s, in general agreement, though somewhat larger in magnitude, than that observed for desorption from bare GaAs. Thus, we interpret the shift as being due to repulsive lateral interactions.

With regard to the differences between the MeS/GaAs(110) and the bare GaAs(110) surfaces, we first note that in the monolayer coverage regime the desorption temperatures are ~ 50 K lower than for the bare GaAs surface, indicating a significant decrease in the strength of the molecule–surface bond due to the insertion of a spacer layer. This is a reasonable result given the electrostatic nature of the binding of MeBr to the (110) GaAs surface.²⁷ The molecule–surface bond is expected to be weaker in the presence of an organic spacer layer for at least three reasons: (1) the spacer layer prevents overlap of the Br lone pair with the Ga *p* orbital, (2) the MeBr–GaAs interaction decreases as the distance between the molecular and Ga–As surface dipoles increases, and (3) the C–H bonds in the methyl moiety at the top of the MeS/GaAs(110) surface have much weaker permanent dipoles than does the GaAs surface.

Further comparison of Figures 4 and 6 and Figure 5a,b reveal a marked qualitative difference between the adsorption on the

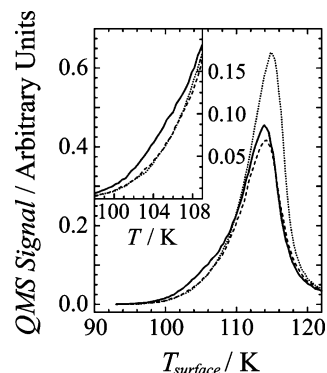


Figure 7. TPD spectra of MeBr from EtS/GaAs(110) at coverages equal to 1.1, 1.2, and 1.5 ML, from bottom to top. (Inset) Enlarged portion of the leading edge of these spectra showing the shoulder at ~ 105 K in the 1.2 ML spectrum suggestive of the presence of a small fraction of a monolayer of second layer admolecules.

bare surface and the functionalized surface. As shown in the inset of Figure 6, as the coverage is increased, instead of a continued, although slower, decrease in the desorption temperature as observed on the bare surface, at ~ 0.6 ML the trend is reversed and the peak desorption temperature begins to increase. Furthermore, the shape of the desorption wave changes. At coverages below ~ 0.6 ML, the desorption wave is roughly symmetric; however, as the coverage is increased, the high-temperature side of the desorption wave takes on the form of a sharp edge, which shifts to higher temperature with increasing coverage. The form and coverage dependence of the higher coverage desorption waves are characteristic of zero-order desorption. In addition, no new desorption features are observed at coverages up to at least 7 ML, consistent with desorption from bulklike three-dimensional (3-D) clusters.

Finally, Figure 7 shows that the leading edge changes its slope between 1.0 and 1.5 ML, exhibiting a slight shoulder at ~ 105 K during desorption of 1.2 ML of MeBr. This subtle behavior was reproduced for each TPD measurement in this coverage regime. Though subtle, we believe it is significant, in particular because it occurs at a coverage very nearly equal to 1 ML. As explained further below, we tentatively attribute this behavior to the transition between the first- and zero-order regimes, which occurs as the coverage just exceeds 1 ML.

The coverage dependence of the desorption behavior can be explained by phase changes in the MeBr layer. Though somewhat speculative, the following scenario explains the qualitative features of the data: At coverages < 0.5 ML, the adsorbed MeBr dipoles are parallel and thus repelling, resulting in a decrease in the desorption-peak temperature with increasing coverage or decreasing intermolecular spacing. This behavior is identical to that on bare GaAs; however, on the bare surface, the decrease is throughout the entire submonolayer range. In contrast, on the MeS-functionalized surface, at coverages > 0.6 ML, the peak temperature of the desorption wave stops shifting to lower temperatures and remains nearly constant until the coverage reaches ~ 1 ML. This is consistent with a change in structure at a coverage of about 0.5 ML. We suggest that this is a result of antiferroelectric ordering of the molecular dipoles into a structure similar to that observed in the **a–b** plane of bulk crystalline MeBr.⁴⁶ Such a structure is consistent with diffraction measurements of MeBr monolayers on LiF(001), NaCl(001), and C(0001).^{18,47,48} This switch to an antiferroelectric ordering at ~ 0.5 ML does not occur on the bare GaAs surface where the overlap of the Br lone pair with the Ga *p* orbital and strong molecular dipole–surface dipole interactions determine

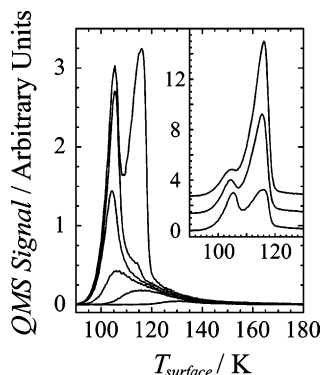


Figure 8. Coverage dependence of the desorption spectra of MeBr from EtS/GaAs(110) in the low-coverage regime. Coverages are 0.01, 0.05, 0.10, 0.20, 0.30, and 0.60 ML, from bottom to top. (Inset) Coverage dependence of the desorption spectra of MeBr from EtS/GaAs(110) at higher coverages. Coverages are: 0.60, 0.91, and 1.22 ML, and spectra are displaced vertically for clarity.

the molecular orientation.²⁷ However, the presence of the spacer layer would prevent the orbital overlap and weaken the dipole interactions sufficiently to allow lateral interactions among adsorbed molecules to dominate at higher coverage. With further increasing coverage, at ~ 1 ML, a second transition occurs, indicated by subtle changes in the leading edge of the desorption curve, which we attribute to second-layer admolecules randomly adsorbed atop the first monolayer with the same structural phase. This structure is supported only over a narrow coverage range, as beyond 1.2 ML, the TPD indicates zero-order desorption, which we attribute to the formation of 3-D clusters.

E. MeBr Adsorption on EtS/GaAs(110). Figure 8 shows measurements of the TPD of MeBr from the surface of a sample prepared with an EtS layer formed by Et₂S₂ chemisorption. TPD spectra, taken as a function of coverage from 0.01 to 1.22 ML, reveal an unusual and unexpected behavior. Namely, at lower coverages (<0.3 ML), a low-temperature peak dominates the spectra, and increasing the coverage results in the formation of a higher-temperature desorption wave. The order of appearance of the low- and high-temperature features is the reverse of what is typically seen, where binding forces are stronger for the first adsorbed layer than they are for second and higher layers. Quantitative consideration of the spectra gives some clue as to the reason for this behavior.

For coverages <0.20 ML, the data show similar desorption behavior as for the MeS/GaAs(110) and bare GaAs(110) surfaces. Specifically, the desorption temperature decreases with coverage, again indicating lateral repulsion in the monolayer due to dipole–dipole interactions among the MeBr molecules. In the EtS/GaAs case, the change in desorption peak temperature with increasing coverage is roughly -200 K/ML, significantly steeper than observed in both the MeS/GaAs(110) and bare GaAs cases, as can be seen in Figure 5. The increased slope may be due to further weakening of the molecule–surface interaction, as the longer ethyl moiety distances the MeBr still farther from the GaAs surface. With increasing coverage, a clear transition occurs at ~ 0.3 ML. This transition is marked by the “pinning” of the temperature of the low-temperature feature at ~ 105 K and the development of the higher temperature feature at ~ 115 K, which becomes more pronounced as the coverage approaches and exceeds 1 ML. The position of this feature increases slightly with coverage, consistent with that observed in the 1–2 ML coverage range in the MeS/GaAs(110) case (Figure 5b). The high-temperature feature similarly exhibits a sharp falling edge, indicative of a zero-order process, likely

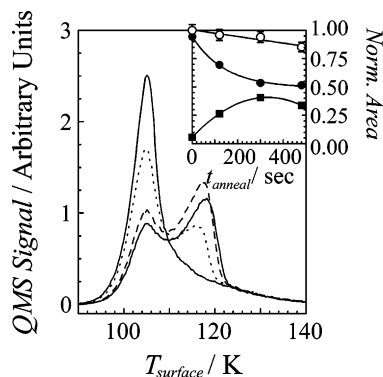


Figure 9. The effect of pre-TPD annealing at 90 K on the TPD spectrum of MeBr from the surface of EtS/GaAs(110). The spectrum consisting of a single high-intensity peak at 105 K is of desorption of an as-deposited MeBr overlayer. The remaining spectra were taken after annealing for 2, 5, and 8 min. (short-dashed, long-dashed, and solid lines, respectively). (Inset) Integrated intensity of the MeBr desorption features: total TPD signal (○), the low-temperature desorption wave (●), and the high-temperature desorption wave (■).

indicating the formation of 3-D clusters. Interestingly, as the coverage increases, the magnitude of the low temperature peak decreases, whereas that of the higher temperature peak concomitantly increases. A plot of the integrated area under the TPD curves vs exposure (data not shown) shows that throughout the entire range of coverage, the integrated TPD signal increases linearly, indicating a constant sticking coefficient. This indicates that with increasing coverage, the high-temperature feature is “borrowing” intensity from the low-temperature feature. Finally, we note that a unity sticking coefficient and stable TPD data for this system are only obtained at temperatures below ~ 80 K, as explained in the following paragraph.

We observed the balance of adsorbate–surface and adsorbate–adsorbate interactions to be particularly delicate in this system. When dosing at our standard LN₂-cooled base crystal temperature of ~ 90 K, we found that the ratio of the intensities of the 105 and 115 K peaks did not remain constant from measurement to measurement. After eliminating possible sources of experimental error, we hypothesized that thermal activation of the molecules could lead to rearrangement over time, even at 90 K. To establish this, we pumped on the cryostat to lower the pressure and thus the boiling point of the LN₂, thereby lowering the surface temperature below 80 K. Repeated TPD measurements following dosing below 80 K yielded reproducible intensity ratios. To confirm that restructuring is thermally activated, we made repeated measurements where 0.3 ML of MeBr was deposited on the EtS/GaAs at <82 K. Prior to performing each TPD measurement, the surface was warmed to 90 K for a set period of time. The results of these measurements are shown in Figure 9. It is immediately obvious from the TPD spectra that annealing causes the high-temperature feature to increase while the low-temperature feature decreases in intensity. In the inset of Figure 9, the behavior of the TPD spectra is quantified in terms of the total integrated intensity under the two waves (○), and the integrated intensity under the low-temperature (●) and high temperature (■) components. This analysis reveals that a relatively small fraction ($\leq 15\%$) of the MeBr desorbs during the 480 s, 90 K anneal, corresponding to a rate of $\sim 1 \times 10^{-4}$ ML per second. In addition, a significant change in the ratio of the two components is observed. Whereas, in the unannealed monolayer there is no evidence of the 115 K desorption wave, with annealing, the ratio of the intensity of the 115 K feature to that of the 105 K feature increases dramatically and appears to approach an equilibrium value of

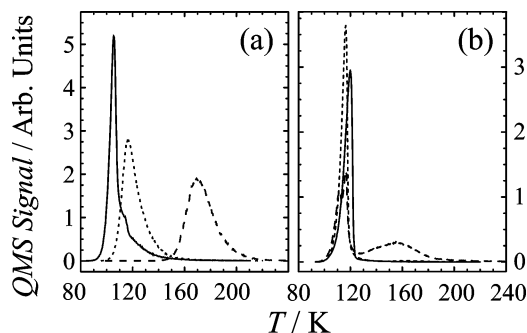


Figure 10. (a) Comparison of desorption of submonolayer MeBr from bare (long-dashed line), MeS-functionalized (short-dashed line), and EtS-functionalized (solid line) GaAs(110) surfaces. The initial MeBr coverage is 0.3 ML. (b) Comparison of desorption of multilayer MeBr from bare, MeS-, and EtS-functionalized GaAs(110) surfaces as in (a), except that the initial MeBr coverage is ~ 2.5 ML.

~ 0.7 . The behavior is consistent with the development of an equilibrium between a submonolayer-coverage phase (105 K peak) and a cluster structure (115 K peak). As the sample is annealed at 90 K, initially, molecules diffuse to form clusters, and the cluster phase grows at the expense of the submonolayer-coverage phase. Simultaneously, there is some desorption from the submonolayer-coverage phase and, possibly, also from the clusters.

Discussion

At least two earlier studies have addressed the issue of the dependence of adsorbate interactions on spacer-layer thickness. In one study, the enthalpy of desorption for three probe molecules, hexane, octane, and dodecane, adsorbed on thiol spacer layers of varying thickness on Au(111) were compared²⁵ and all were found to agree with the bulk heat of vaporization within experimental error—even for a spacer layer as thin as 0.3 nm. This was taken to indicate that the dispersion interaction between the adsorbates and the spacer-layer molecules predominates over the dispersion interaction between the adsorbates and the underlying Au(111), given their short-range nature.²⁵ In a similar vein, SFG measurements were used to probe interactions between various liquids and an oxygen atom “buried” at a depth determined by the length of the alkoxy group at the chain-termini of long-chain alkoxy thiols on gold and silver.²³ This study concluded that as the length of the alkoxy group increased, the effect of the interactions between the oxygen and the molecules of the supernatant liquid rapidly decreased; the butyl–ether-terminated surface was indistinguishable from a simple alkanethiol.²³ Like this study, we have chosen to focus on a molecule–substrate system where dipolar interactions, which are not as short in range as dispersion interactions, are important. Thus, we do not expect to see bulklike adsorbate behavior as was observed in the hydrocarbon–thiol/Au(111) case. On the other hand, we have performed these experiments at low temperature in UHV on short, tightly bound overlayers where we do not expect the adsorbates to greatly perturb the structure of the spacer layer, as was observed in the SFG study.²³

To quantify the degree of the changes in the surface interactions that occur in this short-chain spacer layer limit and begin to understand the structural consequences of these changes, we consider the energetics and kinetics of the desorption process. These may be quantified from our results, which are summarized by the examples of TPD spectra shown in Figure 10. Figure 10a shows that the introduction of an organic spacer layer, or an increase in its thickness, results in a marked

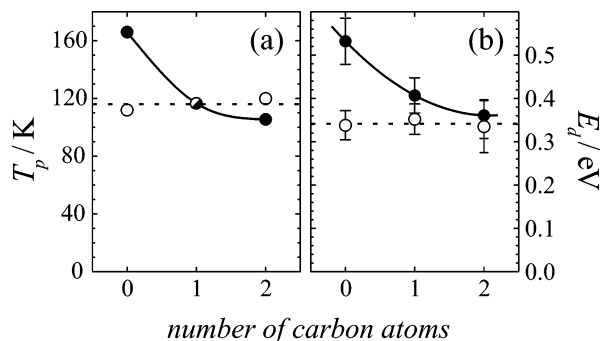


Figure 11. (a) Dependence of the peak MeBr desorption temperature for 0.3 ML (solid line) and 2.5 ML (dashed line) on surface functionalization. (b) The dependence of the activation energy for desorption (as determined by the HK leading edge method) for desorption of 0.3 ML (solid line) and 2.5 ML (dashed line) MeBr on surface functionalization. The lines are simple guides to the eye.

decrease in the temperature of the peak of the desorption wave for the submonolayer (~ 0.3 ML) desorption feature. In contrast, Figure 10b shows that the leading edge of the multilayer (~ 2.5 ML) desorption features remains fairly constant, as expected for a process that follows zero-order kinetics. The positions of the peaks of the desorption waves are plotted in Figure 11a for comparison of the submonolayer and multilayer waves across the three surfaces. We have analyzed the TPD data in Figure 10 using the HK leading-edge analysis³⁷ to obtain the activation energy for desorption versus chain length for both the sub- and multilayer regimes, and the results of this analysis are plotted in Figure 11b. These data show that though the desorption activation energy for MeBr at ~ 2.5 ML coverage on the three surfaces is the same within experimental uncertainty, the desorption activation energy for MeBr from submonolayer coverage shows a distinct trend, decreasing over the series of interfaces; bare GaAs > MeS/GaAs > EtS/GaAs.

There are two important conclusions that can be drawn from the dependence of the desorption activation energies shown in Figure 11b. First, the results for the ~ 2.5 ML coverage cases help confirm our assignment of the ~ 120 K desorption feature, because the activation energy for desorption from bulklike MeBr should be independent of the substrate and in reasonable agreement with the bulk heat of vaporization (0.248 eV).⁴⁹ And second, the variation measured at ~ 0.3 ML represents a significant decrease in the strength of the interaction between the MeBr and the substrate. Most notably, on the EtS-functionalized surface, E_d is lowered to a value roughly equal to that for desorption from 3-D clusters. Thus, the variation in molecule–surface interaction strength is expected to strongly modify the adsorption/desorption behavior in these systems.

Another important conclusion can be gleaned from comparison of the coverage dependence of the TPD spectra presented in Figures 4, 6, and 8. Specifically, the data indicate that the critical coverage required for the formation of bulklike 3-D MeBr (likely in the form of layers in the case of the bare surface and small clusters in the case of the organofunctionalized surfaces) decreases with spacer chain-length. On the bare GaAs(110) surface, distinct desorption features are observed for the first, second, and third monolayer (Figure 4), indicating layer-by-layer growth into the third layer, extending perhaps to higher coverages. However, MeS-functionalization of the surface causes 3-D clustering to occur at the much lower coverage of ~ 1.2 ML, as indicated by subtle changes in the leading edge of the desorption wave (Figure 7), and a switch from first- to zero-order kinetics, as described in the results section. The critical coverage for 3-D cluster formation is decreased further

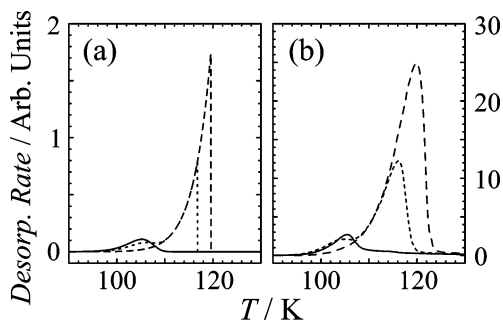


Figure 12. Comparison of the (a) PW model and (b) measured desorption spectra of MeBr from a EtS/GaAs(110) surface. Initial MeBr coverages are 0.3, 1.2, and 2.4 ML (solid, short-dashed, and long-dashed lines, respectively).

by EtS functionalization of the GaAs(110) surface, as indicated by appearance of the multilayer feature at a coverage as low as ~ 0.3 ML (Figure 8). Thus, a decrease in the strength of the molecule–surface interaction decreases the critical coverage for 3-D clustering from ≥ 3 ML, to 1.2 ML, and to 0.3 ML for the bare, MeS-, and EtS-terminated surfaces, respectively.

We attribute this change in behavior to a change from dominating adsorbate–surface attraction toward dominating adsorbate lateral interactions. The change is most dramatically illustrated in the case of the EtS-functionalized surface. Consider the desorption data obtained for MeBr from the EtS/GaAs surface shown in Figures 8 and 10. The most surprising feature of these data is the fact that the peak in the multilayer wave occurs at a temperature higher than that for the submonolayer desorption wave, at coverages as low as 0.3 ML. This is not seen in the case of bare GaAs(110) or MeS/GaAs(110). To further understand this behavior, we employ a *simple* model of the observed desorption processes using a basic rate-equation treatment as given in the Arrhenius expression often called the Polanyi–Wigner (PW) equation,^{34,50}

$$R_d = -d\theta/dt = \nu(\theta) \theta^n \exp[-E_d(\theta)/k_B T] \quad (6)$$

where R_d is the rate of desorption, θ is the surface coverage, t is the time, ν is a preexponential factor (the so-called “frequency factor”), n is the desorption order, E_d is the activation barrier to desorption, k_B is Boltzmann’s constant, and T is the surface temperature. In general, E_d and ν depend on θ . Analysis of TPD data to extract accurate kinetic parameters is far from a trivial task, and development of a comprehensive model for the desorption kinetics is beyond the scope of our considerations here. For example, we note that modeling of the desorption waves is complicated by the effects of the dipole–dipole lateral interactions among the adsorbate molecules that cause the activation energy to depend on coverage.^{26,45} Therefore, our goal in application of the PW rate law here is to establish a semiquantitative basis for the validation of our qualitative understanding of the desorption kinetics and their dependence upon the proposed structure of the MeBr adlayers on EtS/GaAs. A more intensive modeling effort would involve a detailed consideration of lateral interactions and would benefit greatly from direct structural probes of the overlayers.

To model the data, we use the kinetic parameters ν and E_d , extracted from the 0.3- and 2.4-ML spectra shown in Figure 12b, representing coverages where we believe the kinetics to be first- and zero-order, respectively. The HK leading edge method gives the activation energies of desorption for the 0.3- and 2.4-ML spectra to be 0.36 and 0.34 eV, respectively, as shown in Figure 11b. Furthermore, Habenschaden and Küppers

suggested that under the assumptions that E_d and ν are independent of coverage, the preexponential factor can be calculated for a first-order desorption process according to the equation³⁷

$$\nu = \frac{\beta E_p}{k_B T_p^2} \exp\left(\frac{E_p}{k_B T_p}\right) \quad (7)$$

where T_p and E_p are the temperature and desorption activation energy at the peak of the desorption wave, and β is the temperature ramp rate. For a zero-order process, the preexponential factor can be determined from the y -intercept, b , of the $\ln(-d\theta/dT)$ vs T^{-1} Arrhenius plot:

$$\nu = \beta \exp(b) \quad (8)$$

Using the activation energies determined from the leading edge method, we arrive at estimates for the values for the preexponential of $1.7 \times 10^{17} \text{ s}^{-1}$ and $3.7 \times 10^{14} \text{ ML s}^{-1}$ for the 0.3 and 2.4 ML desorption waves. Substituting the E_d and ν into the PW equation, and numerically integrating eq 6 to obtain simulated TPD spectra, we find that both the 0.3- and 2.4-ML desorption waves are quite well reproduced by the PW first- and zero-order models, respectively (Figure 12). The figure also includes a calculation of the 1.2 ML TPD spectrum, using the E_d and ν values determined above and assuming two channels, first- and zero-order, with an integrated intensity fixed at a ratio to approximate that observed in the experiment.

Application of the PW rate law to the interpretation of our results is consistent with our intuitive understanding of the desorption kinetics and their dependence upon the proposed structure of the MeBr adlayers on EtS/GaAs. Specifically, the model helps to explain the somewhat counter-intuitive observation that, in the case of MeBr/EtS/GaAs, the peak in the mono/multilayer desorption wave occurs some 10–20 K *higher* than that for the submonolayer wave, despite the fact that the HK analysis gives an activation energy of desorption for the submonolayer wave that is somewhat greater than that for the mono/multilayer. Our analysis reveals that the reason for this apparent contradiction can be attributed to the different rate laws that govern desorption and the corresponding differing preexponential factors. That the associated preexponentials differ by nearly 3 orders of magnitude is consistent with an adsorbate bound in two distinct states of differing degrees of lateral mobility.^{51,52}

This work has raised the possibility of a number of experiments that could be performed to further our understanding of interfacial molecular interactions. First, detailed and direct structural characterization of organofunctionalized GaAs(110) surfaces, as well as of overlayers adsorbed on their surfaces, using scanning tunneling microscopy, helium atom diffraction, and IR spectroscopy would greatly improve our understanding of these interesting systems and their temperature-dependent behavior. In addition, similar measurements involving other adsorbates would allow for further systematic studies. For example, use of the three common methyl halides, MeI, MeCl, and MeF, would permit studies where the strength of lateral dispersion interactions can be varied while keeping the dipole–dipole interactions roughly constant. Finally, we note that detailed modeling of the TPD spectra and theoretical calculations of the interactions would provide greater insight into the delicate balance of forces that are responsible for the phenomena described here.

Conclusion

The central results here show that slight changes in the chemical composition of small molecules comprising an adsorbed spacer layer in the range of ~ 0.5 nm thick can have major effects on surface adsorption. Classically, such effects have been observed by altering the surface functionality using much more drastic changes in surface functionalization, for example, switching the surface termination of Si from acidic to basic, as in the case of switching from H- to OH-terminated Si, which is known to alter a host of Si surface properties. More recent measurements of this phenomenon have examined more subtle effects by chain-length alterations in molecules on various SAM layers. However, these studies have generally focused on long-chain hydrocarbons and the differences between polar and nonpolar adsorbates. The results shown here are focused on short-chain adlayers in a system where the range of the interaction between the molecule and the underlying substrate appear to be long enough to still be important for a spacer layer comprised of a methyl thiolate moiety. Our measurements show that incrementing the chain length by one methylene unit is sufficient to alter the surface-binding properties of the secondary adsorbate. The changes are significant enough to affect the manner in which the molecular films grow. Such effects could be used, for example, to control the formation of thin-layer structures used in surface modification or reaction processes.

Acknowledgment. N.C. acknowledges the support of the Laboratory Directed Research and Development Program at Brookhaven National Laboratory. This research was carried out in part under contracts DE-FG02-90ER14104 (Columbia) and DE-AC02-98CH10886 (Brookhaven) from the U.S. Department of Energy and also supported by the Office of Basic Energy Sciences.

References and Notes

- (1) Lowndes, D. H. (Chair), Nanoscale Science, Engineering and Technology Research Directions, Basic Energy Sciences Nanoscience/Nanotechnology Group, A report prepared at Oak Ridge National Laboratory for the Office of Basic Energy Sciences, U.S. Department of Energy (http://www.sc.doe.gov/bes/reports/files/NSET_rpt.doc, accessed Jan. 13, 2006.)
- (2) Love, J. C.; Estroff, L. A.; Kriebel, J. K.; Nuzzo, R. G.; Whitesides, G. M. *Chem. Rev.* **2005**, *105*, 1103.
- (3) Sigal, G. B.; Mrksich, M.; Whitesides, G. M. *J. Am. Chem. Soc.* **1998**, *120*, 3464.
- (4) Sanche, L.; Bass, A. D.; Ayotte, P.; Fabrikant, I. I. *Phys. Rev. Lett.* **1995**, *75*, 3568.
- (5) Ayotte, P.; Gamache, J.; Bass, A. D.; Fabrikant, I. I.; Sanche, L. *J. Chem. Phys.* **1997**, *106*, 749.
- (6) Rowntree, P. A.; Olsen, C. *J. Chem. Phys.* **1998**, *108*, 3750.
- (7) Bumm, L. A.; Arnold, J. J.; Dunbar, T. D.; Allara, D. L.; Weiss, P. *J. Phys. Chem. B* **1999**, *103*, 8122.
- (8) Cui, X. D.; Primak, A.; Zarate, X.; Tomfohr, J.; Sankey, O. F.; Moore, A. L.; Moore, T. A.; Gust, D.; Harris, G.; Lindsay, S. M. *Science* **2001**, *294*, 571.
- (9) Sikes, H. D.; Smalley, J. F.; Dudek, S. P.; Cook, A. R.; Newton, M. D.; Chidsey, C. E. D.; Feldberg, S. W. *Science* **2001**, *291*, 1519.
- (10) Chidsey, C. E. D. *Science* **1991**, *251*, 919.
- (11) Shtein, M.; Mapel, J.; Benziger, J. B.; Forrest, S. R. *Appl. Phys. Lett.* **2002**, *81*, 268.
- (12) Gerstenberg, M. C.; Schreiber, F.; Leung, T. Y. B.; Bracco, G.; Forrest, S. R.; Scoles, G. *Phys. Rev. B* **2000**, *61*, 7678.
- (13) Schreiber, F.; Gerstenberg, M. C.; Dosch, H.; Scoles, G. *Langmuir* **2003**, *19*, 10004.

- (14) Huang, L.; Chey, S. J.; Weaver, J. H. *Phys. Rev. Lett.* **1998**, *80*, 4095.
- (15) Antonov, V. N.; Palmer, J. S.; Bhatti, A. S.; Weaver, J. H. *Phys. Rev. B* **2003**, *68*, 205418.
- (16) Kerner, G.; Asscher, M. *Nano Lett.* **2004**, *4*, 1433.
- (17) Horn, J. M.; Song, Z.; Potapenko, D. V.; Hrbek, J.; White, M. G. *J. Phys. Chem. B* **2005**, *109*, 44.
- (18) Rowntree, P. A. Ph.D. Thesis, Princeton University, Princeton, NJ, 1990.
- (19) Engquist, I.; Liedberg, B. *J. Phys. Chem.* **1996**, *100*, 20089.
- (20) Engquist, I.; Parikh, A. N.; Allara, D. L.; Lundstrom, I.; Liedberg, B. *J. Chem. Phys.* **1997**, *106*, 3038.
- (21) Vogt, A. D.; Beebe, T. P., Jr. *Langmuir* **1999**, *15*, 2755.
- (22) Vogt, A. D.; Beebe, T. P., Jr. *J. Phys. Chem. B* **1999**, *103*, 8482.
- (23) Ong, T. H.; Davies, P. B.; Bain, C. D. *Langmuir* **1993**, *9*, 1836.
- (24) Chidsey, C. E. D.; Liu, G.-Y.; Scoles, G.; Wang, J. *Langmuir* **1990**, *6*, 1804.
- (25) Schwartz, P. V.; Lavrich, D. J.; Scoles, G. *Langmuir* **2003**, *19*, 4969.
- (26) Lu, P.-H.; Lasky, P. J.; Yang, Q.-Y.; Wang, Y.; Osgood, R. M., Jr. *J. Chem. Phys.* **1994**, *101*, 10145.
- (27) Black, S.; Friesner, R.; Lu, P.; Osgood, R. *Surf. Sci.* **1997**, *382*, 154.
- (28) Camillone, N., III.; Kahn, K. A.; Osgood, R. M., Jr. *Surf. Sci.* **2000**, *453*, 83.
- (29) Sheen, C. W.; Shi, J.-X.; Mårtensson, J.; Parikh, A. N.; Allara, D. L. *J. Am. Chem. Soc.* **1992**, *114*, 1514; McGuinness, C. L.; Shaporenko, A.; Mars, C. K.; Uppili, S.; Zharnikov, M.; Allara, D. L. *J. Am. Chem. Soc.* **2006**, *128*, 5231.
- (30) Shaporenko, A.; Adlkofer, K.; Johansson, L. S. O.; Ulman, A.; Grunze, M.; Tanaka, M.; Zharnikov, M. *J. Phys. Chem. B* **2004**, *108*, 17964; Adlkofer, K.; Shaporenko, A.; Zharnikov, M.; Grunze, M.; Ulman, A.; Tanaka, M. *J. Phys. Chem. B* **2003**, *107*, 11737.
- (31) Ye, S.; Li, G.; Noda, H.; Uosaki, K.; Osawa, M. *Surf. Sci.* **2003**, *529*, 163.
- (32) Dorsten, J. F.; Maslar, J. E.; Bohn, P. W. *Appl. Phys. Lett.* **1995**, *66*, 1755.
- (33) Schreiber, F. *Prog. Surf. Sci.* **2000**, *65*, 151.
- (34) Redhead, P. A. *Vacuum* **1962**, *12*, 203.
- (35) Camillone, N., III.; Adib, K.; Khan, K. A.; Mocuta, D.; Osgood, R. M., Jr. *J. Phys. Chem. B* **2002**, *106*, 12491.
- (36) Camillone, N., III.; Khan, K. A.; Lasky, P. J.; Wu, L.; Moryl, J. E.; Osgood, R. M., Jr. *J. Chem. Phys.* **1998**, *109*, 8045 and references therein.
- (37) Habenschaden, E.; Küppers, J. *Surf. Sci.* **1984**, *138*, L147.
- (38) Majer, V.; Svoboda, V.; *Enthalpies of Vaporization of Organic Compounds: A Critical Review and Data Compilation*; Blackwell Scientific: Oxford, 1985.
- (39) Kahn, K. A.; Camillone, N., III.; Osgood, R. M., Jr. *J. Phys. Chem.* **1999**, *103*, 5530.
- (40) Kahn, K. A.; Camillone, N., III.; Yarmoff, J. A.; Osgood, R. M., Jr. *Surf. Sci.* **2000**, *458*, 53.
- (41) McMillen, D. F.; Golden, D. M. *Annu. Rev. Phys. Chem.* **1982**, *33*, 493.
- (42) Lavrich, D. J.; Wetterer, S. M.; Bernasek, S. L.; Scoles, G. *J. Phys. Chem. B* **1998**, *102*, 3456.
- (43) Yang, Q. Y.; Schwarz, W. N.; Lasky, P. J.; Hood, S. C.; Loo, N. L.; Osgood, R. M., Jr. *Phys. Rev. Lett.* **1994**, *72*, 3068.
- (44) Lasky, P. J.; Lu, P. H.; Yang, M. X.; Osgood, R. M., Jr.; Bent, B. E.; Stevens, P. A. *Surf. Sci.* **1995**, *336*, 140.
- (45) Maschhoff, B. L.; Cowin, J. P. *J. Chem. Phys.* **1994**, *101*, 8138.
- (46) Kawaguchi, T.; Hijikigawa, M.; Hayafuji, Y.; Ikeda, M.; Fukushima, R.; Tomiie, Y. *Bull. Chem. Soc. Jpn.* **1973**, *46*, 53.
- (47) Rowntree, P. A.; Scoles, G.; Ruiz-Suarez, J. C. *J. Phys. Chem.* **1990**, *94*, 8511.
- (48) Robinson, G. N.; Camillone, N., III.; Rowntree, P. A.; Liu, G.-Y.; Wang, J.; Scoles, G.; *J. Chem. Phys.* **1992**, *96*, 9212.
- (49) Dean, J. A., Ed. *Lange's Handbook of Chemistry*; McGraw-Hill: New York, 1985.
- (50) deJong, A. M.; Niemantsverdriet, J. W. *Surf. Sci.* **1990**, *233*, 355.
- (51) Zhu, X. D.; Rasing, Th.; Shen, Y. R. *Chem. Phys. Lett.* **1989**, *155*, 459.
- (52) Ibach, H.; Erley, W.; Wagner, H. *Surf. Sci.* **1980**, *92*, 29.